

# Modifications for numerical stability of black hole evolution

Hwei-Jang Yo<sup>1,\*</sup>, Chun-Yu Lin<sup>2</sup>, and Zhoujian Cao<sup>3†</sup>

<sup>1</sup>*Department of Physics, National Cheng-Kung University, Tainan 701, Taiwan,*

<sup>2</sup>*National Center for High-Performance Computing, Hsinchu 300, Taiwan*

<sup>3</sup>*Institute of Applied Mathematics, Academy of Mathematics and Systems Science,  
Chinese Academy of Sciences, Beijing 100190, China*

(Dated: November 4, 2018)

We experiment with several new modifications to the Baumgarte-Shapiro-Shibata-Nakamura (BSSN) formulation of Einstein's field equation, and demonstrate how these modifications affect the stability of numerical black hole evolution. With these modifications, we obtain accurate and stable simulations of both single excised Kerr-Schild black holes and punctured binary black holes.

PACS numbers: 04.25.Dm, 04.30.Db, 95.30.Sf, 97.60.Lf

## I. INTRODUCTION

Numerical relativity is aimed at solving Einstein's equations with the aid of computers. It took decades to reformulate Einstein's equations to the required stability and accuracy in simulations. Breakthroughs in 2005 and 2006 [1, 2] brought this development to a more mature status, gave confidence to the community in modeling gravitational wave sources and extracting information of gravitation radiation from the simulations of binary compact objects. Since then, observations in simulations which have been refined and extensively studied over the past few years include long term gravitational waves and the final state of the binary compact objects merger (see review articles [3–5] and reference therein), gravitational recoil of a black hole [6], relativistic jet formation from mergers of black holes [7], and neutron stars [8]. These also provide new insights into mathematical general relativity. Numerical relativity has now become an indispensable and efficient tool in the research of general relativity and astrophysics.

Among the numerous reformulations of Einstein's equations, two particular formulations are most frequently adopted for the simulations of black holes. One of them is the generalized harmonic formulation, in either second-order formulation [1], or fully first-order formulation [9] (In either case the key ingredient for stability of this formulation is a constraint damping mechanism [10]). The other is the Baumgarte–Shapiro–Shibata–Nakamura (BSSN) system [11], which has been implemented by many groups using finite difference codes, in first-order-in-time and second-order-in-space form.

There have been many studies in modifying the BSSN formulation to increase its numerical stability. For example, Alcubierre and Brügmann [12] combined the BSSN formulation with constraints enforcing the traceless condition of the conformal extrinsic curvature in every time step, replacing the conformal connection function  $\tilde{\Gamma}^i$  with

that calculated from the Christoffel symbols whenever  $\tilde{\Gamma}^i$  is undifferentiated. With these modifications, they evolved single black holes in Kerr-Schild coordinates stably with octant grid symmetry, and all fields settled down to equilibrium without encountering any instability. The confinement to grid symmetry was relaxed later in [13], by adding the  $\Gamma$ -constraint to the field equation of  $\tilde{\Gamma}^i$  in order to suppress instability, as well as by employing alternative techniques in the enforcement of other algebraic constraints. Yoneda and Shinkai analyzed analytically the constraint propagation of BSSN formulation in [14], and proposed adjustments to obtain better stability by adding constraint terms. The follow-up work in [15] numerically verified the advantage of their adjustments in stability over the original BSSN formulation. Higher-order derivatives of constraint was also added to the field equation in [16] to enhance stability. A first-order BSSN formulation has been developed in [17] to seek more stable performance in simulations.

In this work, we report numerical tests of new modifications to the BSSN system. The work can be considered as an extended study based on an earlier article [13]. The modifications include (1) adding the  $\Gamma$ -constraint to the field equation of the conformal three-metric; (2) replacing the conformal connection function calculated from the conformal metric, i.e.,  $\tilde{\Gamma}_{\mathbf{g}}^i$ , with the independent  $\tilde{\Gamma}^i$ , and enhancing the derivative of the unimodular determinant constraint in the connection with an irreducible decomposition; (3) applying, with some deformation, the adjustment of the field equation of the conformal extrinsic curvature with the momentum constraint proposed in [14, 15]. We also emphasize the alternative method in [13] in the enforcement of the unimodular constraint and the traceless conformal extrinsic curvature constraint in every timestep. We experiment with these modifications on simulations of single Kerr-Schild black hole, and obtain evolutions with long-term stability. These modifications, also applied to the evolutions of binary punctured black hole, demonstrate better stability and accuracy than the original BSSN formulation against numerical errors, either from finite-differencing or from mesh refinement.

The paper is organized as follows: We summarize the BSSN formulation in Sec. II. Our modifications of the

---

\*Electronic address: hjoyo@phys.ncku.edu.tw

†Electronic address: zjcao@amt.ac.cn

BSSN scheme are described in Sec. III. Single black hole spacetimes in Kerr-Schild coordinates and binary black hole with punctures are described in Sec. IV. We discuss numerical implementations and the gauge conditions in Sec. V. In Sec. VI we present results of our simulations for both single black hole and binary black holes. We summarize and discuss the implications of our findings in Sec. VII. Throughout this paper we adopt geometric units,  $G = c = 1$ .

## II. THE BSSN FORMULATION

The metric in the ADM form is

$$ds^2 = -\alpha^2 dt^2 + \gamma_{ij}(dx^i + \beta^i dt)(dx^j + \beta^j dt), \quad (1)$$

wherein  $\alpha$  is the lapse function,  $\beta^i$  is the shift vector, and  $\gamma_{ij}$  is the spatial three-metric. Throughout this paper, Latin indices are spatial indices and run from 1 to 3, whereas Greek indices are space-time indices and run from 0 to 3.

Einstein's equations can then be decomposed into the Hamiltonian constraint  $\mathcal{H}$  and the momentum constraints  $\mathcal{M}_i$

$$\mathcal{H} \equiv R - K_{ij}K^{ij} + K^2 = 0, \quad (2)$$

$$\mathcal{M}_i \equiv \nabla_j K^j_i - \nabla_i K = 0, \quad (3)$$

and the evolution equations

$$\frac{d}{dt}\gamma_{ij} = -2\alpha K_{ij}, \quad (4)$$

$$\frac{d}{dt}K_{ij} = -\nabla_i \nabla_j \alpha + \alpha(R_{ij} - 2K_{i\ell}K^\ell_j + KK_{ij}). \quad (5)$$

Here we have assumed vacuum  $T_{\alpha\beta} = 0$  and have used

$$\frac{d}{dt} = \frac{\partial}{\partial t} - \mathcal{L}_{\vec{\beta}}, \quad (6)$$

where  $\mathcal{L}_{\vec{\beta}}$  is the Lie derivative with respect to  $\beta^i$ .  $\nabla_i$  is the covariant derivative associated with  $\gamma_{ij}$ ,  $R_{ij}$  is the three-dimensional Ricci tensor

$$R_{ij} = \frac{1}{2}\gamma^{k\ell}(\gamma_{kj,il} + \gamma_{il,kj} - \gamma_{kl,ij} - \gamma_{ij,k\ell}) + \gamma^{k\ell}(\Gamma^m_{i\ell}\Gamma_{mkj} - \Gamma^m_{ij}\Gamma_{mk\ell}), \quad (7)$$

where

$$\Gamma^i_{jk} \equiv \frac{1}{2}\gamma^{i\ell}(\gamma_{\ell j,k} + \gamma_{\ell k,j} - \gamma_{jk,\ell}). \quad (8)$$

And  $R$  is its trace  $R = \gamma^{ij}R_{ij}$ .

In the BSSN formalism [11], the above ADM equations are rewritten by introducing the conformally related metric  $\tilde{\gamma}_{ij}$

$$\tilde{\gamma}_{ij} = e^{-4\phi}\gamma_{ij}, \quad (9)$$

with the conformal exponent  $\phi$  chosen so that the determinant  $\tilde{\gamma}$  of  $\tilde{\gamma}_{ij}$  is unity

$$e^{4\phi} = \gamma^{1/3}, \quad (10)$$

where  $\gamma$  is the determinant of  $\gamma_{ij}$ . The traceless part of the extrinsic curvature  $K_{ij}$ , defined by

$$A_{ij} = K_{\langle ij \rangle} \equiv K_{ij} - \frac{1}{3}\gamma_{ij}K, \quad (11)$$

where  $K_{ij}$  with two indices between  $\langle \rangle$  is to take the symmetric and traceless part of  $K_{ij}$ , and  $K = \gamma^{ij}K_{ij}$  is the trace of the extrinsic curvature, is conformally decomposed according to

$$\tilde{A}_{ij} = e^{-4\phi}A_{ij}. \quad (12)$$

The conformal connection functions  $\tilde{\Gamma}^i$ , initially defined as

$$\tilde{\Gamma}^i \equiv \tilde{\gamma}^{jk}\tilde{\Gamma}^i_{jk} = -\tilde{\gamma}^{ij}_{,j}, \quad (13)$$

are regarded as independent variables in this formulation.

The evolution equations of BSSN formulation can be written as

$$\frac{d}{dt}\phi = -\frac{1}{6}\alpha K, \quad (14)$$

$$\frac{d}{dt}\tilde{\gamma}_{ij} = -2\alpha\tilde{A}_{ij}, \quad (15)$$

$$\frac{d}{dt}K = \alpha\left(\tilde{A}_{ij}\tilde{A}^{ij} + \frac{1}{3}K^2\right) - \nabla^2\alpha, \quad (16)$$

$$\frac{d}{dt}\tilde{A}_{ij} = \alpha(K\tilde{A}_{ij} - 2\tilde{A}_{ik}\tilde{A}^k_j) + e^{-4\phi}(\alpha R_{\langle ij \rangle} - \nabla_{\langle i}\nabla_{j \rangle}\alpha), \quad (17)$$

$$\begin{aligned} \partial_t \tilde{\Gamma}^i &= 2\alpha\left(\tilde{\Gamma}^i_{jk}\tilde{A}^{jk} - \frac{2}{3}\tilde{\gamma}^{ij}K_{,j} + 6\tilde{A}^{ij}\phi_{,j}\right) - 2\tilde{A}^{ij}\alpha_{,j} \\ &\quad + \beta^j\tilde{\Gamma}^i_{,j} - \tilde{\Gamma}^j\beta^i_{,j} + \frac{2}{3}\tilde{\Gamma}^i\beta^j_{,j} + \tilde{\gamma}^{jk}\beta^i_{,jk} + \frac{1}{3}\tilde{\gamma}^{ij}\beta^k_{,jk}. \end{aligned} \quad (18)$$

The Ricci tensor  $R_{ij}$  can be written as a sum of two pieces

$$R_{ij} = \tilde{R}_{ij} + R_{ij}^\phi, \quad (19)$$

where  $R_{ij}^\phi$  is given by

$$R_{ij}^\phi = -2\tilde{\nabla}_i\tilde{\nabla}_j\phi - 2\tilde{\gamma}_{ij}\tilde{\nabla}^2\phi + 4\tilde{\nabla}_i\phi\tilde{\nabla}_j\phi - 4\tilde{\gamma}_{ij}\tilde{\nabla}^k\phi\tilde{\nabla}_k\phi, \quad (20)$$

where  $\tilde{\nabla}_i$  is the covariant derivative with respect to  $\tilde{\gamma}_{ij}$ , while, with the help of the  $\tilde{\Gamma}^i$ ,  $\tilde{R}_{ij}$  can be expressed as

$$\begin{aligned} \tilde{R}_{ij} &= -\frac{1}{2}\tilde{\gamma}^{mn}\tilde{\gamma}_{ij,mn} + \tilde{\gamma}_{k(i}\tilde{\Gamma}^k_{,j)} + \tilde{\Gamma}^k\tilde{\Gamma}_{(ij)k} \\ &\quad + \tilde{\gamma}^{mn}[2\tilde{\Gamma}^k_{m(i}\tilde{\Gamma}_{j)kn} + \tilde{\Gamma}^k_{in}\tilde{\Gamma}_{kmj}]. \end{aligned} \quad (21)$$

The new variables are tensor densities, so that their Lie derivatives are

$$\mathcal{L}_{\tilde{\beta}} K = \beta^k K_{,k}, \quad (22)$$

$$\mathcal{L}_{\tilde{\beta}} \phi = \beta^k \phi_{,k} + \frac{1}{6} \beta^k_{,k}, \quad (23)$$

$$\mathcal{L}_{\tilde{\beta}} \tilde{\gamma}_{ij} = \beta^k \tilde{\gamma}_{ij,k} + 2\tilde{\gamma}_{k(i} \beta^k_{,j)} - \frac{2}{3} \tilde{\gamma}_{ij} \beta^k_{,k}, \quad (24)$$

$$\mathcal{L}_{\tilde{\beta}} \tilde{A}_{ij} = \beta^k \tilde{A}_{ij,k} + 2\tilde{A}_{k(i} \beta^k_{,j)} - \frac{2}{3} \tilde{A}_{ij} \beta^k_{,k}. \quad (25)$$

The Hamiltonian and momentum constraints (2) and (3) can be rewritten as

$$\mathcal{H} = e^{-4\phi} (\tilde{R} - 8\tilde{\nabla}^2 \phi - 8\tilde{\nabla}^i \phi \tilde{\nabla}_i \phi) + \frac{2}{3} K^2 - \tilde{A}_{ij} \tilde{A}^{ij} = 0, \quad (26)$$

$$\mathcal{M}_i = \tilde{\nabla}_j \tilde{A}_i{}^j + 6\phi_{,j} \tilde{A}_i{}^j - \frac{2}{3} K_{,i} = 0, \quad (27)$$

where  $\tilde{R} = \tilde{\gamma}^{ij} \tilde{R}_{ij}$ . Besides being used to obtain the evolution equations (16) and (18) in the BSSN formulation, the Hamiltonian and the momentum constraints are also applied to the volume integrals of the ADM mass and the angular momentum (in vacuum), respectively [18]:

$$M = \frac{1}{16\pi} \oint_{\partial\Omega} (\tilde{\Gamma}^i - 8\tilde{\gamma}^{ij} \partial_j e^\phi) d\tilde{\Sigma}_i \quad (28)$$

$$= \frac{1}{16\pi} \int_{\Omega} [e^{5\phi} (\tilde{A}_{ij} \tilde{A}^{ij} - \frac{2}{3} K^2) + \tilde{\Gamma}^j_{,j} - e^\phi \tilde{R}] d^3x, \quad (29)$$

$$J_i = \frac{1}{8\pi} \epsilon_{ij}{}^k \oint_{\partial\Omega} e^{6\phi} x^j \tilde{A}^k{}_k d\tilde{\Sigma}_\ell \quad (30)$$

$$= \frac{1}{8\pi} \epsilon_{ij}{}^k \int_{\Omega} e^{6\phi} (\tilde{A}^j{}_k + \frac{2}{3} x^j K_{,k} - \frac{1}{2} x^j \tilde{A}_{\ell m} \tilde{\gamma}^{\ell m}{}_{,k}) d^3x, \quad (31)$$

where  $d\tilde{\Sigma}_i = (1/2) \epsilon_{ijk} dx^j dx^k$ . These two global quantities are useful tools for the system diagnostics to validate the calculations.

### III. ADJUSTING THE BSSN EQUATIONS

The BSSN formulation has been described in detail in previous papers [13]. We will discuss here only the new improvements. For a solution of the BSSN equations to be equivalent with a solution of the ADM equations, the new auxiliary variables have to satisfy new constraint equations. In particular, the determinant of the conformally related metric  $\tilde{\gamma}_{ij}$  has to be unity,

$$\mathcal{D} \equiv \tilde{\gamma} - 1 = 0, \quad (32)$$

and  $\tilde{A}_{ij}$  has to be traceless

$$\mathcal{T} \equiv \tilde{\gamma}^{ij} \tilde{A}_{ij} = 0, \quad (33)$$

and the conformal connection functions  $\tilde{\Gamma}^i$  have to satisfy the identity

$$\mathcal{G}^i \equiv \tilde{\Gamma}^i - \tilde{\Gamma}^i_{\mathbf{g}} = \tilde{\Gamma}^i + \tilde{\gamma}^{ij}{}_{,j} = 0, \quad (34)$$

where  $\tilde{\Gamma}^i_{\mathbf{g}} \equiv \tilde{\gamma}^{jk} \tilde{\Gamma}^i{}_{jk}$ . These conditions (32)-(34) are also viewed as constraints in the BSSN formulation, in addition to the Hamiltonian and momentum constraints. It is worth mentioning that in the recent efforts on the formalism extending the solution space of Einstein's equation [19], the  $\mathcal{G}^i$ 's are related to new dynamical variables whose evolution is mainly driven by momentum constraint, and therefore can be regarded as the cumulated effect of momentum constraint violations.

In an unconstrained evolution calculation, the constraints are monitored only as a code check. It has been proven to be advantageous, however, either to enforce at least some of the constraints during the evolution, or to add evolution constraint equations to the evolution equations.

#### A. Enforcement of the constraints $\mathcal{D}$ and $\mathcal{T}$

In the conventional adjustments [12, 20], the algebraic constraints (32) and (33) are enforced actively by replacing  $\tilde{\gamma}_{ij}$  and  $\tilde{A}_{ij}$  with the following:

$$\tilde{\gamma}_{ij} \rightarrow \tilde{\gamma}^{-1/3} \tilde{\gamma}_{ij}, \quad \tilde{A}_{ij} \rightarrow \tilde{A}_{(ij)}, \quad (35)$$

after every time step. With Eq. (35), the noise from the violation of constraints (32) and (33) is scaled/subtracted "evenly" from each conformal metric/extrinsic curvature component. These two adjustments are widely used in most of the numerical relativity groups.

The alternative adjustments for constraints (32) and (33) in [13] are as follows: Instead of treating all components of  $\tilde{\gamma}_{ij}$  equally, only five of the six components of  $\tilde{\gamma}_{ij}$  need to be evolved dynamically, and the remaining one can simply be computed using Eq. (32). For example, let  $\tilde{\gamma}_{zz}$  be the chosen component. Then

$$\tilde{\gamma}_{zz} = \frac{1 + \tilde{\gamma}_{yy} \tilde{\gamma}_{xz}^2 - 2\tilde{\gamma}_{xy} \tilde{\gamma}_{yz} \tilde{\gamma}_{xz} + \tilde{\gamma}_{xx} \tilde{\gamma}_{yz}^2}{\tilde{\gamma}_{xx} \tilde{\gamma}_{yy} - \tilde{\gamma}_{xy}^2}, \quad (36)$$

where  $\tilde{\gamma}_{xx}$ ,  $\tilde{\gamma}_{yy}$ ,  $\tilde{\gamma}_{xy}$ ,  $\tilde{\gamma}_{yz}$ ,  $\tilde{\gamma}_{xz}$  are evolved with the field equation (15). In principle, any one of these six components of  $\tilde{\gamma}_{ij}$  can be chosen to be computed using Eq. (32), leaving the other five to be evolved with Eq. (15). However, there will be extra difficulty if any of the three off-diagonal variables is chosen since Eq. (32) gives a quadratic equation for an off-diagonal component instead of a linear equation for a diagonal component. Similarly, only five of the six components of  $\tilde{A}_{ij}$  need to be evolved dynamically, and the remaining one can simply be computed using Eq. (33). For example, let  $\tilde{A}_{yy}$  be the chosen component. Then

$$\tilde{A}_{yy} = -\frac{\tilde{A}_x{}^x + \tilde{A}_z{}^z + \tilde{A}_{xy} \tilde{\gamma}^{xy} + \tilde{A}_{yz} \tilde{\gamma}^{yz}}{\tilde{\gamma}_{yy}}. \quad (37)$$

Although any one of these six components can be chosen to be computed using Eq. (33), leaving the other five to be evolved with Eq. (17). However, it is not recommended to choose any of the three off-diagonal components since the corresponding denominators for the off-diagonal components, i.e.,  $\tilde{\gamma}^{xy}$ ,  $\tilde{\gamma}^{yz}$ , and  $\tilde{\gamma}^{xz}$ , could vanish anywhere.

One of the features of the alternative adjustments on  $\tilde{\gamma}_{ij}$  and  $\tilde{A}_{ij}$  is the economy compared with conventional methods. Only five, instead of six, components for both  $\tilde{\gamma}_{ij}$  and  $\tilde{A}_{ij}$  need to be evolved dynamically, and the remaining one is determined by the algebraic constraint. Meanwhile, the alternative adjustments “correct” only one component instead of all the components. It can be expected that results with the alternative adjustments will be more convergent than those with conventional adjustments. On the other hand, the obvious shortcoming for the alternative adjustments is the asymmetric treatment of the six components. However, as far as the cases we have ever checked, the effect of the asymmetry is negligible. It is helpful numerically to choose a different diagonal pair for  $\tilde{\gamma}_{ij}$  and  $\tilde{A}_{ij}$ , instead of the same diagonal pair, in eqns (36) and (37) to increase the asymmetry in the evolution equations and to suppress the possible growth of the unstable modes ignited by numerical error. In the work we choose the pair  $(\tilde{\gamma}_{zz}, \tilde{A}_{yy})$ , instead of  $(\tilde{\gamma}_{zz}, \tilde{A}_{zz})$  in [13], to fulfill this requirement.

## B. Decomposition

For a third-rank tensor  $Y_{ijk}$  with symmetry in the last two indices, i.e.,  $Y_{ijk} = Y_{i(jk)}$ , it can be decomposed into the following form [21]

$$Y_{ijk} = \mathbb{Y}_{ijk} + \frac{3}{5}\gamma_{i(j}L_{k)} - \frac{1}{5}\gamma_{i(j}Y_{k)} + \frac{1}{3}\gamma_{jk}Y_i, \quad (38)$$

where

$$L_i \equiv \gamma^{jk}Y_{jki} = \gamma^{jk}Y_{jik}, \quad Y_i \equiv \gamma^{jk}Y_{ijk}, \quad (39)$$

and  $\mathbb{Y}_{ijk}$  is the traceless part of  $Y_{ijk}$ , i.e.,  $\mathbb{Y}_{ik}{}^k = \mathbb{Y}^k{}_{ik} = \mathbb{Y}^k{}_{ki} = 0$ . We can apply the decomposition (38) to the connection in *every* time slice although a connection is not a tensor. The is because any quantity can be decomposed like a tensor as long as the quantity is only considered in the same coordinate, without any coordinate transformations involved. Thus the conformal connection can be decomposed as

$$\tilde{\Gamma}^i{}_{jk} = \tilde{F}^i{}_{jk} + \frac{3}{5}\delta^i{}_{(j}\tilde{T}_{k)} - \frac{1}{5}\delta^i{}_{(j}\tilde{\Gamma}_{k)}^{\mathbf{g}} + \frac{1}{3}\tilde{\gamma}_{jk}\tilde{\Gamma}^i{}_{\mathbf{g}}, \quad (40)$$

where  $\tilde{T}_i \equiv \tilde{\Gamma}^k{}_{ki} = \tilde{\Gamma}^k{}_{ik}$ , and  $\tilde{F}^i{}_{jk}$  is the traceless part of  $\tilde{\Gamma}^i{}_{jk}$ . Here  $\tilde{T}_i = \tilde{\Gamma}^k{}_{ki} = \partial_i \ln \sqrt{\tilde{\gamma}} = 0$  analytically, but  $\tilde{T}_i$  could be nonzero numerically due to the truncation error. We can guarantee the vanishing of  $\tilde{T}_i$  by subtracting the terms having it from Eq. (40).  $\tilde{\Gamma}_{\mathbf{g}}^i$  in Eq. (40) can be

replaced with the conformal connection function  $\tilde{\Gamma}^i$  by adding the  $\Gamma$ -constraint to it. Then the new connection becomes

$$\begin{aligned} \tilde{T}^i{}_{jk} &= \tilde{\Gamma}^i{}_{jk} - \frac{3}{5}\delta^i{}_{(j}\tilde{T}_{k)} - \frac{1}{5}\delta^i{}_{(j}\mathcal{G}_{k)} + \frac{1}{3}\tilde{\gamma}_{jk}\mathcal{G}^i \\ &= \tilde{F}^i{}_{jk} - \frac{1}{5}\delta^i{}_{(j}\tilde{\Gamma}_{k)} + \frac{1}{3}\tilde{\gamma}_{jk}\tilde{\Gamma}^i. \end{aligned} \quad (41)$$

We substitute  $\tilde{\Gamma}^i{}_{jk}$  with the new one  $\tilde{F}^i{}_{jk}$  in all the calculations, including the conformal covariant derivatives and the conformal Ricci tensor, as a new modification.

Similarly, the spatial derivative of the conformal metric can also be decomposed in every time slice as

$$\partial_i \tilde{\gamma}_{jk} = \overline{\partial}_i \tilde{\gamma}_{jk} + \frac{3}{5}\tilde{\gamma}_{i(j}\tilde{\Gamma}_{k)}^{\mathbf{g}} - \frac{1}{5}\tilde{\gamma}_{i(j}T_{k)} + \frac{1}{3}\tilde{\gamma}_{jk}T_i, \quad (42)$$

where  $\overline{\partial}_i \tilde{\gamma}_{jk}$  is the traceless part of  $\partial_i \tilde{\gamma}_{jk}$ . We use the same trick on the conformal connection part like we did on Eq. (41) and obtain a new spatial derivative on  $\tilde{\gamma}_{ij}$

$$d'_i \tilde{\gamma}_{jk} = \partial_i \tilde{\gamma}_{jk} + \frac{3}{5}\tilde{\gamma}_{i(j}\mathcal{G}_{k)}. \quad (43)$$

Here we do not take action on eliminating the  $T^i$  part in Eq. (42) since its effect is negligible from the observation of our numerical experiment.

However, it turns out that this replacement of the spatial derivative of the conformal metric seems give too much change on the field equation of  $\tilde{\gamma}_{ij}$  and causes in instability when  $d'_i \tilde{\gamma}_{jk}$  is applied in Eq. (24). This problem can be solved when the modification (56) in Sec. III D is applied in simulations, at least in single black hole simulations. Nevertheless, we modify Eq. (43), by multiplying an adjustable parameter to the substitution part, to have

$$d_i \tilde{\gamma}_{jk} = \partial_i \tilde{\gamma}_{jk} + \sigma \tilde{\gamma}_{i(j}\mathcal{G}_{k)} - \frac{1}{5}\tilde{\gamma}_{jk}\mathcal{G}_i, \quad (44)$$

where the range of the parameter is usually chosen as  $\sigma \in [1/5, 4/5]$  in this work. And

$$\beta^i d_i \tilde{\gamma}_{jk} = \beta^i \partial_i \tilde{\gamma}_{jk} + \sigma \beta_{(j}\mathcal{G}_{k)} - \frac{1}{5}\tilde{\gamma}_{jk}\beta^i \mathcal{G}_i. \quad (45)$$

Thus the replacement of  $\beta^i \partial_i \tilde{\gamma}_{jk}$  in Eq. (24) with  $\beta^i d_i \tilde{\gamma}_{jk}$  is equivalent to modifying Eq. (15) into

$$\frac{d}{dt} \tilde{\gamma}_{ij} = -2\alpha \tilde{A}_{ij} + \sigma \beta_{(i}\mathcal{G}_{j)} - \frac{1}{5}\tilde{\gamma}_{ij}\beta^k \mathcal{G}_k. \quad (46)$$

We postpone the modification on the field equation of  $\tilde{A}_{ij}$  with the decomposition of the spatial derivative of  $\tilde{A}_{ij}$  until Sec. III D.

## C. Enforcement of the $\Gamma$ -constraint

In the conventional adjustments, to enforce constraint (34) all the undifferentiated  $\tilde{\Gamma}^i$  in the evolution equations

are substituted with  $\tilde{\Gamma}_{\text{g}}^i$ . However, this adjustment give stability in single Kerr-Schild black hole simulations only in octant symmetry [12]. Instead of the conventional adjustment, one of the alternative adjustments [13] (dubbed as ‘‘YBS’’) is to add the  $\Gamma$ -constraint to the evolution equation (18) of  $\tilde{\Gamma}^i$  by

$$\partial_t \tilde{\Gamma}^i = \text{rhs of (18)} - \frac{2}{3}(\xi + 1)\mathcal{G}^i \beta^k{}_{,k}, \quad (47)$$

where  $\xi$  is usually chosen to be unity. The YBS adjustment has been proven to be helpful in suppressing the instability caused from some unstable modes [13, 22].

Here we propose another adjustment to enhance the stability. This adjustment is basically the following substitution in Eq. (18):

$$\tilde{\gamma}^{ij} K_{,j} \rightarrow \kappa^{ij}{}_{,j} + K \tilde{\Gamma}^i, \quad (48)$$

where  $\kappa^{ij} \equiv \tilde{\gamma}^{ij} K$ . And this adjustment turns Eq. (18) into

$$\begin{aligned} \partial_t \tilde{\Gamma}^i &= 2\alpha(\tilde{\Gamma}^i{}_{jk} \tilde{A}^{jk} - \frac{2}{3}\kappa^{ij}{}_{,j} + 6\tilde{A}^{ij} \phi_{,j}) - 2\tilde{A}^{ij} \alpha_{,j} \\ &+ \beta^j \tilde{\Gamma}^i{}_{,j} - \tilde{\Gamma}^j \beta^i{}_{,j} + \tilde{\gamma}^{jk} \beta^i{}_{,jk} + \frac{1}{3} \tilde{\gamma}^{ij} \beta^k{}_{,jk} \\ &+ \frac{2}{3}(\beta^k{}_{,k} - 2\alpha K) \tilde{\Gamma}^i. \end{aligned} \quad (49)$$

As we will show in Sec. VI, the performance of the code with this adjustment is better than the one with the YBS adjustment, but without the uncertainty of choosing the value of the parameter  $\xi$ . Furthermore, the connection in Eq. (49) can be replaced with the new connection  $\tilde{\Gamma}^i{}_{jk}$ , and thus Eq. (49) is modified into

$$\begin{aligned} \partial_t \tilde{\Gamma}^i &= 2\alpha(\tilde{\Gamma}^i{}_{jk} \tilde{A}^{jk} - \frac{2}{3}\kappa^{ij}{}_{,j} + 6\tilde{A}^{ij} \phi_{,j}) - 2\tilde{A}^{ij} \alpha_{,j} \\ &+ \beta^j \tilde{\Gamma}^i{}_{,j} - \tilde{\Gamma}^j \beta^i{}_{,j} + \tilde{\gamma}^{jk} \beta^i{}_{,jk} + \frac{1}{3} \tilde{\gamma}^{ij} \beta^k{}_{,jk} \\ &+ \frac{2}{3}(\beta^k{}_{,k} - 2\alpha K) \tilde{\Gamma}^i - (1 + \xi) \Theta(\lambda^i) \lambda^i \mathcal{G}^i, \end{aligned} \quad (50)$$

where the last term is newly added to control the stability via the linear term of  $\tilde{\Gamma}^i$ ,  $\Theta$  is a step function, and  $\lambda^i$  is as follows:

$$\lambda^i = \frac{2}{3}(\beta^k{}_{,k} - 2\alpha K) - \beta^{\hat{i}}{}_{,\hat{i}} - \frac{2}{5}\alpha \tilde{A}_{\hat{i}}{}^{\hat{i}}, \quad (51)$$

where the index with hat, i.e.,  $\hat{i}$ , means that no index summation happens on this index.  $\xi$  is chosen to be 1 in all the cases in this work.

#### D. Application of the momentum constraint

Yoneda & Shinkai have studied the adjusted systems for the BSSN formulation in [14]. It shown in the work that the adjusted BSSN system could be quite robust

with the following modification on the field equation (17) of  $\tilde{A}_{ij}$  :

$$\frac{d}{dt} \tilde{A}_{ij} = \text{rhs of (17)} + \kappa_A \alpha \tilde{\nabla}_{(i} \mathcal{M}_{j)}, \quad (52)$$

where  $\kappa_A$  is a constant. If  $\kappa_A$  is set as positive, the violations of the constraints are expected to be damped. The robustness of this  $\tilde{A}$ -adjusted BSSN formulation has been demonstrated in [15, 16]. Here we would like to apply this type of modification to the BSSN formulation in a slightly different manner. In the momentum constraint, the covariant derivative of  $\tilde{A}_{ij}$  can be rewritten as

$$\tilde{\nabla}_j \tilde{A}_i{}^j = \tilde{A}_i{}^j{}_{,j} - \tilde{\Gamma}^{kj}{}_i \tilde{A}_{kj} = \tilde{A}_i{}^j{}_{,j} - \frac{1}{2} \tilde{\gamma}^{jk} \tilde{A}_{jk,i}. \quad (53)$$

Thus the momentum constraint turns to be

$$\mathcal{M}_i = \tilde{A}_i{}^j{}_{,j} - \frac{1}{2} \tilde{\gamma}^{jk} \tilde{A}_{jk,i} + 6\phi_{,j} \tilde{A}_i{}^j - \frac{2}{3} K_{,i}. \quad (54)$$

And the symmetric part of its spatially partial derivative is

$$\begin{aligned} \mathcal{M}_{(i,j)} &= \tilde{A}_{(i}{}^k{}_{,j)k} + \tilde{\Gamma}^{k\ell}{}_{(i} \tilde{A}_{k\ell,j)} - \frac{1}{2} \tilde{\gamma}^{k\ell} \tilde{A}_{k\ell,ij} \\ &+ 6\phi_{,k(i} \tilde{A}_{j)k} + 6\phi_{,k} \tilde{A}_{(i}{}^k{}_{,j)} - \frac{2}{3} K_{,ij}. \end{aligned} \quad (55)$$

Therefore, the modification on Eq. (17) in this work is

$$\frac{d}{dt} \tilde{A}_{ij} = \text{rhs of (17)} + hf(\alpha) \mathcal{M}_{(i,j)}, \quad (56)$$

where  $h$  is the grid width and  $f(\alpha)$  is a function of lapse and usually chosen to be 1 in single black hole simulations. It shows in our numerical experiments that this modification is helpful in suppressing the instability from the high-frequency unstable modes.

As in Sec. III B, the spatial derivative of  $\tilde{A}_{ij}$  can be decomposed in every time slice as

$$\partial_i \tilde{A}_{jk} = \overline{\partial_i \tilde{A}_{jk}} + \frac{3}{5} \tilde{\gamma}_{i(j} P_{k)} - \frac{1}{5} \tilde{\gamma}_{i(j} Q_{k)} + \frac{1}{3} \tilde{\gamma}_{jk} Q_i, \quad (57)$$

where  $\overline{\partial_i \tilde{A}_{jk}}$  is the traceless part of  $\partial_i \tilde{A}_{jk}$  and

$$P_i = \tilde{\gamma}^{jk} \partial_j \tilde{A}_{ki}, \quad Q_i = \tilde{\gamma}^{jk} \partial_i \tilde{A}_{jk}. \quad (58)$$

With the momentum constraint (54) and the traceless extrinsic curvature constraint (33), we obtain a new spatial derivative on  $\tilde{A}_{ij}$

$$d_i \tilde{A}_{jk} = \partial_i \tilde{A}_{jk} - \frac{3}{5} \tilde{\gamma}_{i(j} \mathcal{M}_{k)} - \frac{1}{10} \tilde{\gamma}_{i(j} \mathcal{A}_{k)} - \frac{1}{3} \tilde{\gamma}_{jk} \mathcal{A}_i, \quad (59)$$

where  $\mathcal{A}_i$  is the spatially secondary constraint of Eq. (33)

$$\mathcal{A}_i = \partial_i \mathcal{T} = \tilde{\gamma}^{jk} \tilde{A}_{jk,i} + \tilde{A}_{jk} \tilde{\gamma}^{jk}{}_{,i} = Q_i - 2\tilde{A}_{jk} \tilde{\Gamma}^{jk}{}_i = 0. \quad (60)$$

With the new spatial derivative (59), we can modify the field equation of  $\tilde{A}_{ij}$  further from Eq. (56) to

$$\begin{aligned} \frac{d}{dt} \tilde{A}_{ij} &= \text{rhs of (17)} + hf(\alpha) \mathcal{M}_{(i,j)} - \frac{3}{5} \beta_{(i} \mathcal{M}_{j)} \\ &- \frac{1}{10} \beta_{(i} \mathcal{A}_{j)} - \frac{1}{3} \tilde{\gamma}_{ij} \beta^k \mathcal{A}_k. \end{aligned} \quad (61)$$

## IV. INITIAL DATA

### A. Single black hole in Kerr-Schild coordinates

The ingoing Kerr-Schild form of the Kerr metric is given by [23, 24]

$$ds^2 = (\eta_{\mu\nu} + 2H\ell_\mu\ell_\nu)dx^\mu dx^\nu, \quad (62)$$

where  $\eta_{\mu\nu} = \text{diag}(-1, 1, 1, 1)$  is the Minkowski metric in Cartesian coordinates, and  $H$  a scalar function. The vector  $\ell_\mu$  is null both with respect to  $\eta_{\mu\nu}$  and  $g_{\mu\nu}$ ,

$$\eta^{\mu\nu}\ell_\mu\ell_\nu = g^{\mu\nu}\ell_\mu\ell_\nu = 0, \quad (63)$$

and we have  $\ell_i^2 = \ell^k\ell_k$ . The general Kerr-Schild black hole metric has

$$H = \frac{Mr}{r^2 + a^2 \cos^2 \theta} \quad (64)$$

and

$$\ell_\mu = \left(1, \frac{rx + ay}{r^2 + a^2}, \frac{ry - ax}{r^2 + a^2}, \frac{z}{r}\right). \quad (65)$$

Here  $M$  is the mass of the Kerr black hole,  $a = J/M$  is the specific angular momentum of the black hole, and  $r$  and  $\theta$  are auxiliary spheroidal coordinates defined in terms of the Cartesian coordinates by

$$\frac{x^2 + y^2}{r^2 + a^2} + \frac{z^2}{r^2} = 1 \quad (66)$$

and  $z = r \cos \theta$ . The event horizon of the black hole is located at

$$r_{\text{eh}} = M + \sqrt{M^2 - a^2}. \quad (67)$$

Comparing (62) with the ADM metric (1) one identifies the lapse function  $\alpha$ , shift vector  $\beta_i$  and the spatial 3-metric  $\gamma_{ij}$  as

$$\alpha = \frac{1}{\sqrt{1 + 2H}}, \quad (68)$$

$$\beta_i = 2H\ell_i, \quad (69)$$

$$\gamma_{ij} = \eta_{ij} + 2H\ell_i\ell_j. \quad (70)$$

We can see here that these variables all extend smoothly through the horizon and their gradients near the horizon are well-behaved. Given these metric quantities, the extrinsic curvature  $K_{ij}$  can be computed from (4)

$$K_{ij} = 2\alpha H \ell^k [\ell_i \ell_j H_{,k} + 2H \ell_{(i} \ell_{j),k}] + 2\alpha [\ell_{(i} H_{,j)} + H \ell_{(i,j)}], \quad (71)$$

$$K = 2\alpha^3 (1 + H) \ell^k H_{,k} + 2\alpha H \ell^k_{,k}. \quad (72)$$

In the static case  $a = 0$ , the above expressions reduce to the Schwarzschild expressions in ingoing Eddington-Finkelstein form [25]

$$H = \frac{M}{r}, \quad \ell_\mu = \left(1, \frac{x_k}{r}\right),$$

$$K_{ij} = \frac{2M}{r^4(1 + 2M/r)^{1/2}} \left[ r^2 \eta_{ij} - \left(2 + \frac{M}{r}\right) x_i x_j \right], \quad (73)$$

$$K = \frac{2M}{r^2(1 + 2M/r)^{3/2}} \left(1 + 3\frac{M}{r}\right),$$

where  $M$  is the total mass-energy and  $r^2 = x^2 + y^2 + z^2$ .

### B. Binary black hole with punctures

We use the quasi-circular binary black hole puncture data to test our modifications. The momentum parameter for the quasi-circular orbit is set to be the value given by [26] based on the helical Killing vector conditions. In the following, we review the puncture scheme and describe how we construct initial data by the multi-domain spectral method extended from the LORENE library [27, 28].

To determine a three-geometry subject to the constraint equations (2) and (3), the conformal decomposition plays an important role (see [29] for instance). Lichnerowicz [30] proposed a conformal decomposition of three-metric  $\gamma_{ij} = \psi^4 \tilde{\gamma}_{ij}$ , as Eq. (9) with  $\psi = e^\phi$ , and later York [31] used the transverse-traceless decomposition of the conformal extrinsic curvature  $\hat{A}^{ij} \equiv \psi^{10} A^{ij} = \hat{A}_{TT}^{ij} + \tilde{\mathbb{L}}W^{ij}$ . The particular conformal scaling makes the identity  $\nabla_i A^{ij} = \psi^{-10} \tilde{\nabla}_i \hat{A}^{ij}$  hold. In this decomposition,  $\hat{A}_{TT}^{ij}$  is transverse (i.e.,  $\tilde{\nabla}_i \hat{A}_{TT}^{ij} = 0$ ) and can be assumed to be zero to have a purely longitudinal  $\hat{A}^{ij} = \tilde{\mathbb{L}}W^{ij}$ . In this approach, named as conformal transverse-traceless method (CTT), and in the assumption of conformal flatness,  $\tilde{\gamma}_{ij} = \eta_{ij}$ , maximal slicing,  $K = 0$ , and  $\hat{A}_{TT}^{ij} = 0$ , the vacuum constraint equation would then be expressed as

$$\tilde{\nabla}^2 \psi = -\frac{1}{8} \psi^{-7} \hat{A}_{ij} \hat{A}^{ij}, \quad (74)$$

$$\tilde{\nabla}_j \hat{A}^{ij} = 0. \quad (75)$$

The momentum constraint is linear in this case. For a  $N$ -black hole system, it allows the Bowen-York solution  $\hat{A}^{ij} = \sum_{a=1}^N \hat{A}_a^{ij}$ , where the conformal extrinsic curvature for each black hole is [32]

$$\hat{A}_a^{ij} \equiv \psi^{10} A_a^{ij} = \frac{3}{4r^2} [P^{(i} n^{j)} - 2(\gamma^{ij} - n^i n^j) P_k n^k] + \frac{3}{2r^3} n^{(i} \epsilon^{j)k\ell} S_k n_\ell, \quad (76)$$

with  $n^i$  the spatial unit vector pointing away from the puncture, and  $P^i$  and  $S^i$  its linear and intrinsic angular momentum respectively. The conformal factor then can be numerically solved from the Hamiltonian constraint.

TABLE I: Input parameters and modifications used for selected evolutions. For each evolution we list the symmetry used, the method for constraints  $\mathcal{D}$  &  $\mathcal{T}$  enhancement, the modifications on the field equations of  $\tilde{\Gamma}^i$  and  $\tilde{\gamma}_{ij}$ , the substitution of connection, the modification on the field equations of  $\tilde{A}_{ij}$ , the time when instability shows.

Case	Symmetry	$\tilde{\gamma}_{zz} + \tilde{A}_{yy}$	$\tilde{\Gamma}^i$	$\tilde{\gamma}_{ij}$	$\tilde{\Gamma}^i{}_{jk}$	$\tilde{A}_{ij}$	Instability
Eqn		(36)+(37)	(50)	(46)	(41)	(61)	appears at
STD	Equ	(35)	$\tilde{\Gamma}_{\mathbf{g}}^i$				$\sim 250M$
YBS	Equ	✓	(47)				$\sim 650M$
E1	Equ	✓	(49)				$\sim 550M$
E2	Equ	✓	(49)	$\sigma=2/5$			$\sim 750M$
E3	Equ	✓	✓	$\sigma=2/5$	✓		$\sim 850M$
E4	Equ	✓	✓	$\sigma=2/5$	✓	(56)	$\sim 950M$
E5	Equ	✓	✓	$\sigma=3/5$	✓	(56)	None
E6-lo	Equ	✓	✓	$\sigma=3/5$	✓	✓	None
E6	Equ	✓	✓	$\sigma=3/5$	✓	✓	None
E6-hi	Equ	✓	✓	$\sigma=4/5$	✓	✓	None
N7	None	✓	✓	$\sigma=3/5$	✓	✓	None

In the puncture method, one separates out the singular part

$$\psi_s = 1 + \sum_{a=1}^N \frac{m_a}{2r_a}, \quad (77)$$

from the conformal factor  $\psi$ , where  $m_a$  and  $r_a$  are the mass parameter and coordinate distance from each puncture respectively. It is the superposition of Schwarzschild solution in the isotropic coordinate and satisfies the Laplace equation [33]. Therefore the desired regular part  $u \equiv \psi - \psi_s$  is determined by

$$\tilde{\nabla}^2 u = -\frac{1}{8} \hat{A}^{ij} \hat{A}_{ij} (\psi_s + u)^{-7}. \quad (78)$$

The existence and uniqueness of the solution has been discussed in [34].

Our multi-puncture initial data solver is motivated from [35] for the excised binary black hole initial data. We cover on each black hole a spherical multi-shell domain, and split  $u = \sum_a u_a$  (the index  $a$  runs over the number of the black holes) as well as the puncture equation (78) into

$$\tilde{\nabla}^2 u_a = -\frac{1}{8} \hat{A}_a^{ij} \hat{A}_{ij} (\psi_s + u)^{-7}. \quad (79)$$

Only one of the extrinsic curvature tensor  $\hat{A}_{ij}$  split in the above equation. Thus it is expected that the source term in its RHS has large contribution only near each hole, and the use of spherical polar coordinates is adequate for solving the equation near the punctures. The  $u_a$  vanished at the asymptotically flat physical outer boundary on the outermost, compactified shell. And  $\partial_r u_a(r=0) = 0$  is also ensured at the punctures as the inner boundary condition. These equations for each hole are then solved iteratively with the Poisson solver in the LORENE library

until each successive difference of  $\delta u_a$  is small, typically  $10^{-11}$ . For the binary case, our initial data is consistent with the earlier work [36]. The convergence of our method was presented in [37].

## V. NUMERICAL IMPLEMENTATION

In this work, we discretize the evolution equations using a fourth-order Runge-Kutta scheme. We use fourth-order centered differencing everywhere except for the advection terms on the shift. For these terms, a fourth-order upwind scheme is used along the shift direction.

For the lapse gauge condition, we consider the “1+log” slicing [38–40] which is basically a modification of the Bona-Massó slicing. The lapse condition used in the single Kerr-Schild black hole evolutions is

$$\partial_t \alpha = D_i \beta^i - \alpha K. \quad (80)$$

For binary black hole simulations, the moving puncture technique is adopted. And the lapse condition used here is the standard one in numerical relativity community for binary black hole simulation as

$$\partial_t \alpha = \beta^i \alpha_{,i} - 2\alpha K. \quad (81)$$

Many driver gauge conditions (e.g., the  $\Gamma$ -driver) for the shift vector [41, 42] are currently the main type of gauge conditions used in the punctured black hole calculations. In this work, we will only focus on these types of gauge conditions. The hyperbolic type  $\Gamma$ -driver condition used for the single black hole simulations is

$$\partial_t \beta^i = \frac{3}{4} B^i, \quad (82)$$

$$\partial_t B^i = \alpha^2 \partial_t \tilde{\Gamma}^i - \eta B^i, \quad (83)$$

where  $\eta$  is the parameters to be chosen. In the single Kerr-Schild black hole evolutions,  $\eta = 5$ . For the binary black hole simulations, we use

$$\partial_t \beta^i = \frac{3}{4} B^i + \beta^j \beta^i{}_{,j}, \quad (84)$$

$$\partial_t B^i = \partial_t \tilde{\Gamma}^i - 2B^i + \beta^j B^i{}_{,j} - \beta^j \tilde{\Gamma}^i{}_{,j}. \quad (85)$$

On the outer boundaries of the numerical grid we impose a radiative boundary condition that is imposed on the difference between a given variable and its analytic value  $f - f_{\text{analytic}} = u(r-t)/r$  where  $u$  is an outgoing wave function. We apply this condition to all fields except  $\tilde{\Gamma}^i$  which we leave fixed to their analytic values at the boundary in the single Kerr-Schild black hole evolutions for stability. We return to apply the radiative boundary condition on  $\tilde{\Gamma}^i$  in the punctured binary black hole evolutions.

The excision technique is applied in the single Kerr-Schild black hole evolutions since the singularities in the Kerr-Schild coordinates are physical ones for which the puncture method is not applicable. (Usually the puncture method is applied to the isotropic-like coordinates in which the singularities are coordinate ones.) For (spherical) excision regions, we adopt the recipe suggested by [12, 13] to copy the time derivative of every field at the boundary from its neighboring grid-point. The details can be found in [13].

## VI. NUMERICAL RESULT

### A. Single black hole

Our simulations for single Kerr-Schild black holes are summarized in Table I. For most of these simulations we use computational domains of size  $-12M < x, y < 12M$  and  $0 < z < 12M$  for equatorial symmetry, and  $-12M < x, y, z < 12M$  for no symmetry, with a grid spacing of  $\Delta x = 0.2M$ . In order to analyze the effect of resolution we performed the two Cases E6-lo and E6-hi on the same domain and used a resolution of  $\Delta x = 0.4M$  for E6-lo and  $\Delta x = 0.1M$  for E6-hi. We always use a Courant factor of 1/4 so that  $\Delta t = \Delta x/4$ . We excise spheres of radius  $r = 1.6M$  inside the event horizons ( $r = 2M$ ) in these simulations.

A simulation can be judged as being stable if changes in all dynamical variables drop to round-off error (of about  $10^{-16}$  for double precision), and remain at that level as the simulation goes. Reaching round-off implies that the numerical solution has settled down to the equilibrium solution of the finite-difference equations (as opposed to the equilibrium solution of the differential equations, which is provided as initial data). In all our stable runs, besides monitoring the global quantities consisting of the ADM mass (28, 29), the angular momentum  $J_z$  (30,31), the  $L_2$  norms of the Hamiltonian constraint  $\mathcal{H}$ , the momentum constraint  $\mathcal{M}^x$ , and the  $\Gamma$ -constraint  $\mathcal{G}^x$

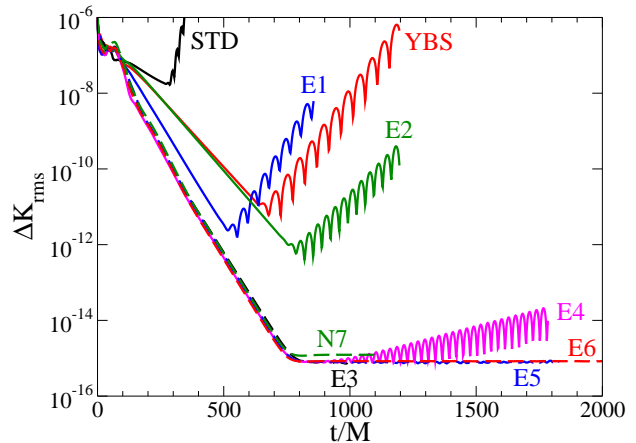


FIG. 1: The root mean square (rms) of the change in the trace of extrinsic curvature between consecutive time steps as functions of time for the cases listed in Table I. The usual BSSN formulation is used in Case STD. The modifications suggested in [13] are used in Case YBS. The modifications suggested in this work are activated one by one from Case E1 to Case E6. Case E5 has the same modifications with Case E4 except with a different value of  $\sigma$  used in Eq. (46). Case N7 has the same modifications with Case E6 except with none symmetry for the computational domain. There is no instability shown in Cases E5, E6, and N7 throughout these runs.

violations, we also monitor the changes in the representative variables, i.e.,  $\phi$ ,  $K$ ,  $\tilde{\gamma}_{xx}$ ,  $\tilde{A}_{xx}$ ,  $\tilde{\Gamma}^x$ ,  $\alpha$ , and  $\beta^x$ , to see if they can reach and remain at the level of round-off error. Due to the existence of singularity inside the excision area, we only consider the domain outside the excision (including the part inside the horizon) for the estimate of the error norm and the changes.

In Fig. 1 we summarize the listed cases with the medium resolution in Table I. As shown in [12, 13], in Case STD the evolution with the usual standard recipes applied to the BSSN formulation becomes unstable quickly. The root mean square (rms) of the changes in  $K$  between consecutive time steps,  $\Delta K_{\text{rms}}$ , in this case drops exponentially until  $t \sim 250M$ , then at later times it increases exponentially. This exponentially growing mode can be extrapolated back to about round-off error at  $t = 0$ , indicating that the mode is triggered by round-off error in the initial data. In Case YBS the recipes suggested in [13], including mainly Eqs. (36,37), and Eq. (47), are applied to the BSSN formulation. Undoubtedly, the evolution in Case YBS is more stable than the one in Case STD. We can see it from that the  $\Delta K_{\text{rms}}$  in this case drops exponentially until  $t \sim 650M$  before it turns to increase exponentially. In fact, the recipes used in Case YBS have been shown in [13] to be able to stabilize an evolution until its  $\Delta K_{\text{rms}}$  reaches round-off error. However, a lower grid resolution and the second-order finite differencing methods both spatially and temporally



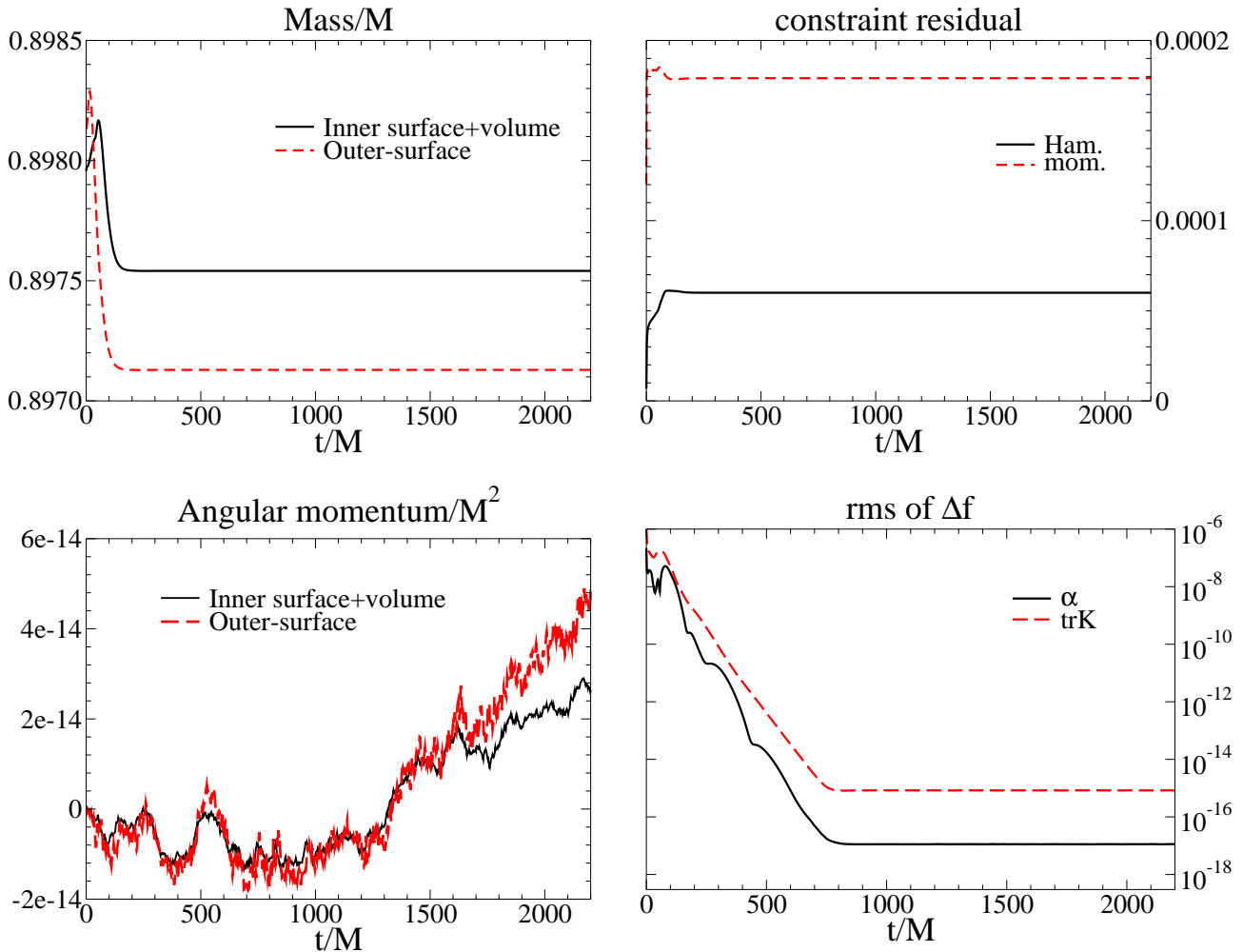


FIG. 2: The monitored quantities as functions of time for Case E6. The upper-left panel compares different integrals for the ADM mass. The lower-left panel compares different integrals for the angular momentum. The upper-right panel shows the L2 norms of the Hamiltonian constraint  $\mathcal{H}$  and the momentum constraint  $\mathcal{M}^x$ . The lower-right panel shows a log plot of the rms of the changes in the lapse and the trace of extrinsic curvature between consecutive time steps.

are used in those numerical experiments. The instability shown in Case YBS indicates that higher-frequency unstable modes triggered with higher grid resolution and/or higher-order finite differencing methods need to be tamed with further modifications to the BSSN formulation.

We test our new modifications from Case E1 to Case E6. In Case E1, the field Eq. (49) for  $\tilde{\Gamma}^i$ , instead of Eq. (47) in Case YBS, is employed in the evolution. As described in Sec. III C, this modification is to enhance the effect of the linear terms in the field equation of  $\tilde{\Gamma}^i$  on convergence and stability. We can see from the plot that the evolution in Case E1 converges faster than the one in Case YBS, and thus encounters the growth of instability from round-off error earlier ( $t \sim 550M$ ). Besides the modifications employed in Case E1, we add the modified field Eq. (46) of  $\tilde{\gamma}_{ij}$  in Case E2 with the parameter choice  $\sigma = 2/5$ . In our numerical experience, this modification is a critical one among the new modifications on

the stability of an evolution. The choice of the parameter  $\sigma$  could also affect the behavior of convergence. From Fig. 1 we can see that the evolution in Case E2 does not show any instability until  $t \sim 750M$ . In Case E3, the connection  $\tilde{\Gamma}^i_{jk}$  is substituted by the new one,  $\tilde{\Gamma}^i_{jk}$ , via the application of Eq. (41). The purpose of the modification is to substitute  $\tilde{\Gamma}^i_{\mathbf{g}}$ , a decomposition part of  $\tilde{\Gamma}^i_{jk}$ , in  $\tilde{\Gamma}^i_{jk}$  with the independent conformal connection  $\tilde{\Gamma}^i$ , as well as enhancing the secondary constraint  $\tilde{\Gamma}^j_{ij} \simeq 0$ . We can see in Fig. 1 that the combination of the modifications used in Case E3 enhances quite a lot the stability of an evolution. The evolution does not show any instability until  $t \sim 850M$  and the  $\Delta K_{\text{rms}}$  reaches almost round-off error before the unstable mode appears.

However, we found that the modifications used in Case E3 are sensitive to the grid resolution. This leads us to employ the modification (56) in Cases E4 and E5. Eq. (56) is adopted from [14] with some deformation.

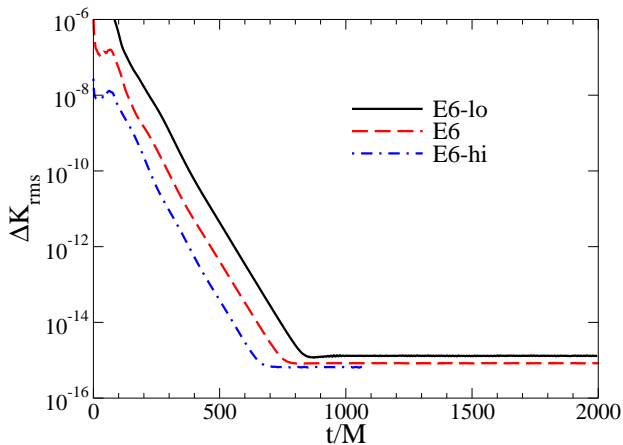


FIG. 3: The rms of the change in the trace of extrinsic curvature between consecutive time steps as functions of time with different resolutions.

This modification offers a dissipation effect on  $\tilde{A}_{ij}$  which fits into our requirement for stability. With this modification, the evolution in Case E4 does not show instability until  $t \sim 950M$  with  $\Delta K_{\text{rms}}$  near round-off error. We push the stability in Case E5 by setting the parameter used in Eq. (46) to be  $\sigma = 3/5$ . Then the  $\Delta K_{\text{rms}}$  and all the other changes drop exponentially until they reach round-off error in Case E5. In Case E6, the modification (61) instead of Eq. (56) is employed. This modification gives a little faster convergence. The settings in Case N7 are the same as in Case E6 except there is not any grid symmetry in N7. This case is used to test the effect of the grid symmetry on the stability of an evolution with the modifications. It shows in Case N7 no sign of instability with the relaxation of symmetry.

Now we would like to look closer at the stable case, i.e., Case E6. The results for Case E6 are presented in Fig. 2. The upper-left panel shows two different integrations of the ADM masses. The (red) dashed line is computed from a surface integral (28) at large separation, while the solid line is computed from a volume integral (29) plus a surface integral over a small sphere enclosing the black hole singularity. We choose a radius of  $R_1 = 2M$  for the inner surface and  $R_2 = 11M$  for the outer surface. For  $R_2 \rightarrow \infty$  the two mass integrals should agree and should yield the analytic value  $M$  of the initial data. Our two mass integrals agree to within about 0.05%. The lower-left panel in Fig. 2 shows surface and volume integrations of the angular momentum, similar to the mass integrations explained above. The (red) dashed line is computed from the outer surface integral (30); the solid line is computed from a combination of volume integral (31) and inner surface integral. For both integrations the angular momentum is very close to zero, as it is supposed to be. These results indicate that the global quantities are consistent with the expected values in single BH and

are not sensitive to the existence of the excision (as long as inside the BH horizon).

The upper-right panel shows the L2 norms of the Hamiltonian constraint  $\mathcal{H}$  (solid line) and the momentum constraint  $\mathcal{M}^x$  (red-dashed line). The lower-right panel shows a log plot of the rms of the changes in the lapse  $\alpha$  (solid line) and the trace of extrinsic curvature  $K$  (red dashed line) between consecutive time steps. The changes in  $\alpha$  and  $K$  both decrease exponentially until they reach round-off error at about  $t \sim 800M$ . We then continue to run the numerical simulation for this case till the time being over  $2000M$  and there is not any sign of instability.

In Fig. 3, we compare the results of Cases E6's using the same modifications but with different resolutions to test the convergence of the formulations. From the plot we can see that in all the three cases the  $\Delta K_{\text{rms}}$ 's reach the round-off errors. The cases for the low and the medium resolutions are extended over  $2000M$ . The case for the high resolution is terminated at  $t \approx 1100M$  due to its time-consuming computation. In Case E6-hi we use  $\sigma = 4/5$ , instead of  $\sigma = 3/5$  in Cases E6-lo and E6, to enhance the stability against higher frequency noise. The results of these three cases indicate a nice convergence with these modifications.

## B. Binary black hole with punctures

We use our numerical code AMSS-NCKU, which has been employed in several previous studies [18, 43, 44]. With this code the standard moving box style mesh refinement is implemented. We used 11 mesh levels in all, where 8 levels are fixed and 3 levels are movable. For fixed levels we used one box with grids  $144 \times 144 \times 72$  where we have taken the advantage of equatorial symmetry of the system. The outermost physical boundary is set to 517.12. For movable levels, two boxes are used. And every box has grids  $72 \times 72 \times 36$ . In time direction, the Berger-Oliger numerical scheme is adopted for levels higher than 4. Although our code can adopt the Kreiss-Oliger numerical dissipation, we *disable* it in order to check the accuracy and stability of our new modification. We set  $\sigma = 0.1$  in Eq. (46) and  $f(\alpha) = h\alpha$  in Eq. (56).

In this subsection both the usual BSSN formalism and our modification are tested and compared with each other, without the Kreiss-Oliger numerical dissipation for both formalisms. Several typical configurations of binary black hole listed in the QC sequence of [45] are tested. We find that, for QC1 and QC2, both formulations give stable and consistent results for whole inspiral and merger phases. However, for QC3 and QC6, both formulations crash at almost the same time moment. We suspect that the failure mainly comes from the numerical error being too much. Compared with the tests in the previous subsection, there is one more complicated numerical issue, that is, the numerical noise introduced by mesh refine-

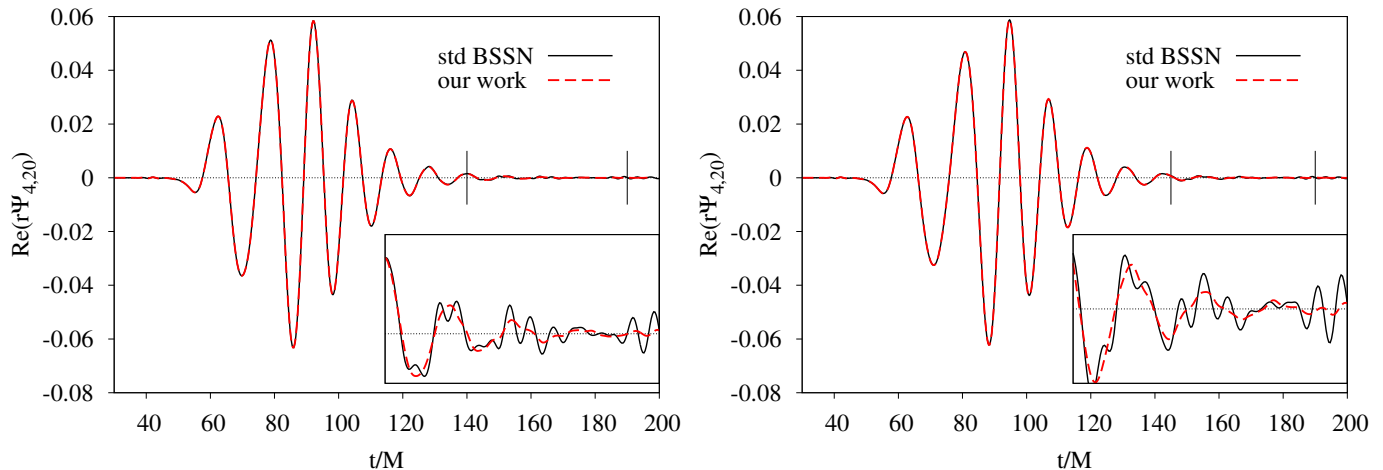


FIG. 4: Comparison of  $\ell = 2, m = 2$  mode of  $\Psi_4$  for the usual BSSN formulation and the one with our new modification. The outermost boundary locates at 517.12. And the detector locates at  $R = 50$ . The (red) dashed line corresponds to the result with our new modification and the solid line corresponds to the result with the usual BSSN formulation. The results from the two formulations are quite consistent. But for the late ringdown phase, shown in the enlarged subplots, our new modification gives a much smoother result.

ment. And this type of noise causes the numerical instability dominantly when the mesh refinement technique is employed during the simulations. Compared with the numerical noise by the discretization of the field equations, the numerical noise induced by mesh refinement is much larger such that the modification is not able to suppress it in time. So in such kind of cases the advantage of our modification on stability does not prevail.

Interestingly we do find our new modification has the advantage on accuracy compared with the usual BSSN formulation. The advantage is manifest on the gravitational radiation wave form calculation. And this issue has been investigated in [44, 46]. As we have mentioned, both the usual BSSN formulation and our new modification are stable for simulations of QC1 and QC2. For completeness, here we list the initial parameters for QC1 and QC2 here. The initial positions of binary black hole for these two configurations are  $(0, \pm 1.364, 0)$  and  $(0, \pm 1.516, 0)$ . The initial linear momentum are  $(\mp 0.286, 0, 0)$  and  $(\mp 0.258, 0, 0)$ . For both configurations the two black holes are spineless and identical with puncture mass parameter 0.463 and 0.47 respectively. We plot the resulted waveform in Fig.4. The waveform is measured by Newman-Penrose quantity  $\Psi_4$ . Our calculation follows the description in [18]. The figure shows that the two formulations give consistent waveform. And the consistence convinces us the new modification does work well for binary black hole simulations. In particular, the formulation with our modification suppresses the numerical error more effectively and produce a smoother waveform than the usual BSSN formulation does during the ring-down phase. We should emphasize that the boundary effects has no effect on the late-time behavior of waveform. Since the outermost boundary is at 517.12 and the waveform is measured at  $R = 50$ , therefore the noise in

the waveform mainly comes from the evolution itself.

## VII. SUMMARY

We experiment with various modifications of the BSSN formulation and study their effects on the stability of numerical evolution calculations of single black hole. Based on the modifications in [13], we enhance the unimodular determinant constraint with Eq. (36) and the traceless extrinsic curvature constraint with Eq. (37). We further modify the evolution equation for the conformal connection functions into Eq. (49) by enhancing the linear term of  $\tilde{\Gamma}^i$ . With an irreducible decomposition (38), we replace the component  $\tilde{\Gamma}_{\mathbf{g}}^i$  in the connection with the  $\tilde{\Gamma}^i$  and enhance the spatial secondary unimodular determinant constraint  $\tilde{\Gamma}^j{}_{ij} = 0$  to form a new connection  $\tilde{\Gamma}^i{}_{ij}$  in Eq. (41). Meanwhile, the field equation of  $\tilde{\Gamma}^i$  is adapted from Eq. (49) into Eq. (50) for the new connection and to ensure the suppression ability of numerical error in its linear term. With the irreducible decomposition on  $\tilde{\gamma}_{ij,k}$ , the field equation of the conformal metric is modified into Eq. (46) by adding the  $\Gamma$ -constraint. The field equation of the conformal extrinsic curvature is modified into Eq. (61) by combining the  $\tilde{A}$ -adjustment proposed in [14] and the irreducible decomposition on  $\tilde{A}_{ij,k}$ .

We found that these modifications on the BSSN formulation do show their superiority on numerical error suppression compared with the earlier work when applied to single Kerr-Schild black hole calculations and thus increase the accuracy eventually. When applied to the binary black hole calculations with the typical initial data and without the Kreiss-Oliger dissipation, the modified BSSN formulation gives a consistent and more accurate result than the conventional method.

Among these modifications, Eq. (46) seems play a key role in stability and thus the whole evolution is quite sensitive to the value of the parameter  $\sigma$ . We suspect that this modification, combined with the Ricci curvature in the field equation of  $\tilde{A}_{ij}$ , could change the characteristic of  $\tilde{\Gamma}^i$ , and thus of the system. However, a further analytic/numerical study is needed to have a better understanding of the effect of this modification.

In this work, we only demonstrate the advantage of these modifications to stability and accuracy of binary black hole simulations without any systematic study on the optimal choice of the related parameters. Thus we plan to address this problem in more detail in a separate upcoming work to increase the numerical accuracy

of future binary black hole simulations.

### Acknowledgments

This work was supported in part by the National Science Council under the grants NSC98-2112-M-006-007-MY2 and NSC100-2112-M-006-005, and by the National Center of Theoretical Sciences. Z. Cao was supported by the NSFC (No. 11005149). We are grateful to the National Center for High-performance Computing for computer time and facilities, and Academia Sinica Computing Center for providing computing resource. We also thank C. Soo for his helpful suggestions and comments.

- 
- [1] F. Pretorius, Phys. Rev. Lett. **95**, 121101 (2005).  
 [2] M. Campanelli, C.O. Lousto, P. Marronetti, and Y. Zlochower, Phys. Rev. Lett. **96**, 111101 (2006); J.G. Baker, J. Centrella, D. Choi, M. Koppitz, and J. van Meter, *ibid.*, 111102 (2006).  
 [3] L. Lehner, Class. Quant. Grav. **18**, R25 (2001).  
 [4] J. Centrella, J.G. Baker, B.J. Kelly, and J.R. van Meter, Rev. Mod. Phys. **82**, 3069 (2010); I. Hinder, Class. Quant. Grav. **27**, 114004 (2010); S.T. McWilliams, *ibid.* **28**, 134001 (2011).  
 [5] T.W. Baumgarte and S.L. Shapiro, Phys. Rept. **376**, 41, (2003); M.D. Duez, Class. Quant. Grav. **27**, 114002 (2010).  
 [6] M. Campanelli, C.O. Manuela, Y. Zlochower, and D. Merritt, Phys. Rev. Lett. **98**, 231102 (2007); M. Koppitz, D. Pollney, C. Reisswig, L. Rezzolla, J. Thornburg, P. Diener, and E. Schnetter, *ibid.* **99**, 041102 (2007); C.O. Lousto and Y. Zlochower, Phys. Rev. D **77**, 044028 (2008); C.O. Lousto and Y. Zlochower, *ibid.* **83**, 024003 (2011); Y. Zlochower, M. Campanelli, and C.O. Lousto, Class. Quant. Grav. **28**, 114015 (2011); C.O. Lousto, Y. Zlochower, M. Dotti, and M. Volonteri, arXiv:1201.1923.  
 [7] J.C. McKinney and R.D. Blandford, arXiv:0812.1060; C. Palenzuela, L. Lehner, and S.L. Liebling, Science **329**, 927 (2010); P. Moesta, D. Alic, L. Rezzolla, O. Zanotti, and C. Palenzuela, Astrophys. J. **749**, L32 (2012).  
 [8] L. Rezzolla, B. Giacomazzo, L. Baiotti, J. Granot, C. Kouveliotou, and M.A. Aloy, Astrophys. J. **732**, L6 (2011).  
 [9] L. Lindblom, M.A. Scheel, L.E. Kidder, R. Owen, and O. Rinne, Class. Quant. Grav. **23**, S447 (2006).  
 [10] O. Brodbeck, S. Frittelli, P. Huebner, and O.A. Reula, J. Math. Phys. **40**, 909 (1999); C. Gundlach, J.M. Martin-Garcia, G. Calabrese, and I. Hinder, Class. Quant. Grav. **22**, 3767 (2005).  
 [11] M. Shibata and T. Nakamura, Phys. Rev. D **52**, 5428 (1995); T.W. Baumgarte and S.L. Shapiro, *ibid.* **59**, 024007 (1999).  
 [12] M. Alcubierre and B. Brügmann, Phys. Rev. D **63**, 104006 (2001).  
 [13] H.J. Yo, T.W. Baumgarte, and S.L. Shapiro, Phys. Rev. D **66**, 084026 (2002).  
 [14] G. Yoneda and H. Shinkai, Phys. Rev. D **66**, 124003 (2002).  
 [15] K. Kiuchi and H. Shinkai, Phys. Rev. D **77**, 044010 (2008).  
 [16] T. Tsuchiya, G. Yoneda, and H. Shinkai, Phys. Rev. D **85**, 044018 (2012).  
 [17] J.D. Brown *et al.*, arXiv:1202.1038.  
 [18] Z. Cao, H.J. Yo, and J.P. Yu, Phys. Rev. D **78**, 124011 (2008).  
 [19] C. Bona, T. Ledvinka, and C. Palenzuela, Phys. Rev. D **66**, 084013(2002); C. Bona, T. Ledvinka, C. Palenzuela, and M. Zacek, *ibid.* **67**, 104005 (2003).  
 [20] P. Laguna and D. Shoemaker, Class. Quant. Grav. **19**, 3679 (2002).  
 [21] Y.N. Obukhov, E.J. Vlachynsky, W. Esser, and F.W. Hehl, arXiv:gr-qc/9705039.  
 [22] U. Sperhake, Phys. Rev. D **76**, 104015 (2007).  
 [23] R.A. Matzner, M.F. Huq, and D. Shoemaker, Phys. Rev. D **59**, 024015 (1999).  
 [24] S. Chandrasekhar, *The Mathematical Theory of Black Holes* (Oxford University Press, New York, 1992).  
 [25] A.E. Eddington, Nature **113**, 192 (1924); D. Finkelstein, Phys. Rev. **110**, 965 (1958).  
 [26] W. Tichy and B. Brügmann, Phys. Rev. D **69**, 024006 (2004).  
 [27] E. Gourgoulhon, P. Grandclément, K. Taniguchi, J. Marck, and S. Bonazzola, Phys. Rev. D **63**, 064029 (2001); K. Taniguchi and E. Gourgoulhon, *ibid.* **66**, 104019 (2002); *ibid.* **68**, 124025 (2003).  
 [28] <http://www.lorene.obspm.fr/>  
 [29] G.B. Cook, Living Rev. Relativity **3**, 5 (2000); E. Gourgoulhon, J. Phys.: Conf. Ser. **91**, 012001 (2007).  
 [30] A.P. Lichnerowicz, J. Math. Pures Appl. **23**, 37 (1944)  
 [31] J.W. York, Phys. Rev. Lett. **26**, 1656 (1971); J.W. York, J. Math. Phys. **14**, 456 (1973); N. Ó Murchadha and J.W. York, Phys. Rev. D **10**, 428 (1974).  
 [32] J.M. Bowen and J.W. York, Phys. Rev. D **21**, 2047 (1980).  
 [33] D.R. Brill and R.W. Lindquist, Phys. Rev. **131**, 471 (1963).  
 [34] S. Brandt and B. Brügmann, Phys. Rev. Lett. **78**, 3606 (1997).  
 [35] E. Gourgoulhon, P. Grandclément, and S. Bonazzola, Phys. Rev. D **65**, 044020 (2002); P. Grandclément, E. Gourgoulhon, and S. Bonazzola, *ibid.*, 044021 (2002).

- [36] M. Ansorg, B. Brügmann, and W. Tichy, Phys. Rev. D **70**, 064011 (2004).
- [37] Z. Cao, J.P. Yu, C.Y. Lin, S. Bai, and H.J. Yo, arXiv:1203.6185
- [38] C. Bona, J. Masso, E. Seidel, and J. Stela, Phys. Rev. Lett. **75**, 600 (1995).
- [39] A. Arbona *et al.*, Phys. Rev. D **60**, 104014 (1999).
- [40] M. Alcubierre *et al.*, Phys. Rev. D **62**, 044034 (2000).
- [41] J. Meter, J. Baker, M. Koppitz and, D. Choi, Phys. Rev. D **73**, 124011 (2006).
- [42] J. Balakrishna, G. Daues, E. Seidel, W. Suen, M. Tobias, and E. Wang, Class. Quant. Grav. **13**, L135 (1996).
- [43] P. Galaviz, B. Brügmann, and Z. Cao, Phys. Rev. D **82**, 024005 (2010).
- [44] Z. Cao and D. Hilditch, arXiv:1111.2177.
- [45] J. Baker, M. Campanelli, C. Lousto, and R. Takahashi, Phys. Rev. D **65**, 124012 (2002).
- [46] D. Alic, C. Bona-Casas, C. Bona, L. Rezzolla, and C. Palenzuela, arXiv:1106.2254.